

Impact of Hydrogen Embrittlement on Minimum Pressurization Temperature for Thick-wall Cr-Mo Steel Reactors in High-pressure H₂ Service—Initial Technical Basis for RP 934-F

API TECHNICAL REPORT 934-F, PART 1
FIRST EDITION, SEPTEMBER 2017



AMERICAN PETROLEUM INSTITUTE

Currently in preview, click buy full version

Impact of Hydrogen Embrittlement on Minimum Pressurization Temperature for Thick-wall Cr-Mo Steel Reactors in High-pressure H₂ Service—Initial Technical Basis for RP 934-F

API TECHNICAL REPORT 934-F, PART 1
FIRST EDITION, OCTOBER 2017

Prepared under contract for API by:

Dr. Richard P. Gangloff
Emeritus Ferman W. Perry Professor of Materials Science and Engineering
Department of Materials Science and Engineering
School of Engineering and Applied Science
University of Virginia, Charlottesville, Virginia



AMERICAN PETROLEUM INSTITUTE

Special Notes

API publications necessarily address problems of a general nature. With respect to particular circumstances, local, state, and federal laws and regulations should be reviewed.

Neither API nor any of API's employees, subcontractors, consultants, committees, or other assignees make any warranty or representation, either express or implied, with respect to the accuracy, completeness, or usefulness of the information contained herein, or assume any liability or responsibility for any use, or the results of such use, of any information or process disclosed in this publication. Neither API nor any of API's employees, subcontractors, consultants, or other assignees represent that use of this publication would not infringe upon privately owned rights.

API publications may be used by anyone desiring to do so. Every effort has been made by the Institute to assure the accuracy and reliability of the data contained in them; however, the Institute makes no representation, warranty, or guarantee in connection with this publication and hereby expressly disclaims any liability or responsibility for loss or damage resulting from its use or for the violation of any authorities having jurisdiction with which this publication may conflict.

API publications are published to facilitate the broad availability of proven, sound engineering and operating practices. These publications are not intended to obviate the need for applying sound engineering judgment regarding when and where these publications should be utilized. The formulation and publication of API publications is not intended in any way to inhibit anyone from using any other practices.

Any manufacturer marking equipment or materials in conformance with the marking requirements of an API standard is solely responsible for complying with all the applicable requirements of that standard. API does not represent, warrant, or guarantee that such products do in fact conform to the applicable API standard.

Users of this technical report should not rely exclusively on the information contained in this document. Sound business, scientific, engineering, and safety judgment should be used in employing the information contained herein.

Copyright reserved. No part of this work may be reproduced, translated, stored in a retrieval system, or transmitted by any means, electronic, mechanical, photocopying, recording, or otherwise, without prior written permission from the publisher. Contact the Publisher, API Publishing Services, 1220 L Street, NW, Washington, DC 20005.

Foreword

Nothing contained in any API publication is to be construed as granting any right, by implication or otherwise, for the manufacture, sale, or use of any method, apparatus, or product covered by letters patent. Neither should anything contained in the publication be construed as insuring anyone against liability for infringement of letters patent.

Questions concerning the interpretation of the content of this publication should be directed in writing to the Director of Standards, American Petroleum Institute, 1220 L Street, NW, Washington, DC 20005. Requests for permission to reproduce or translate all or any part of the material published herein should also be addressed to the director.

Generally, API standards are reviewed and revised, reaffirmed, or withdrawn at least every five years. A one-time extension of up to two years may be added to this review cycle. Status of the publication can be ascertained from the API Standards Department, telephone (202) 682-8000. A catalog of API publications and materials is published annually by API, 1220 L Street, NW, Washington, DC 20005.

Suggested revisions are invited and should be submitted to the Standards Department, API, 1220 L Street, NW, Washington, DC 20005, standards@api.org.

Currently in preview, click buy full version

Contents

	Page
Executive Summary	xii
1 Background	1
2 Problem Statement	8
3 Objective and Scope	10
4 Acronyms and Abbreviations	4
5 Technical Analysis	11
6 Conclusions	92
Bibliography	94
Figures	
1 Effect of loading format on: (top) the threshold for IHAC and (bottom) the growth rate vs stress intensity factor relationship for a modern pure 2¼Cr-1Mo steel containing 5 wppm predissolved H ($C_{H-Total}$) and stressed at 23 °C	2
2 The effect of measured predissolved total H concentration ($C_{H-Total}$) on K_{IH} for the onset of IHAC under rising CMOD ($dK/dt = 0.007 \text{ MPa}\sqrt{\text{m}}$) for laboratory step-cooled 2¼Cr-1Mo base plate and weld metal of several purity levels and tested at 23 °C	3
3 The effect of test temperature on K_{IH} for the onset of IHAC under rising CMOD ($dK/dt = 0.007 \text{ MPa}\sqrt{\text{m}}$) for 2¼Cr-1Mo base plate and weld metal of moderate purity and a single $C_{H-Total}$ of 5 wppm	3
4 The slotted compact tension specimen developed in Phase II for laboratory characterization of K_{IH} and da/dt vs K for IHAC without H loss	5
5 Crack growth rate vs applied stress intensity for the slotted compact tension specimens of 2¼Cr-1Mo weld metal stressed under slow-rising CMOD at 25 °C	6
6 Effect of temperature on the rising CMOD threshold, K_{IH} , for standard H ₂ -precharged specimens of 2¼Cr-1Mo weld metal from Figure 3, as well as for the slotted compact tension specimen with three levels of electrochemically added total H concentration; 3.0 wppm (0.5 M H ₂ SO ₄ + 10 ⁻³ M K ₂ SO ₄ , -5.0 mA/cm ²), 1.8 wppm (0.1 M NaOH, -5 mA/cm ²), and 1.1 wppm (0.5 M H ₂ SO ₄ , -10 mA/cm ²) on the slot surface	6
7 Effect of applied dK/dt , during rising CMOD, on K_{IH} for low-J factor base plate and both low and moderate XB factor weld metal of 2¼Cr-1Mo steel, containing either 5 wppm or 3 wppm of precharged H ($C_{H-Total}$) and stressed at 23 °C	7
8 An example of the intended pressurization vs temperature profile for safe-reactor startup, with the MPT of 150 °C established to minimize the likelihood of both catastrophic fracture due to temper embrittlement and subcritical crack propagation due to IHAC	8
9 Critical temperature for IHAC vs total dissolved H concentration, predicted specifically for a compact tension specimen fabricated from moderate-purity (“High Impurity”) 2¼Cr-1Mo weld metal	9
10 Correlation between measured K_{IH} vs model-predicted concentration of H, trapped along the crack path with a binding energy, E_B , of 38 kJ/mol and in the crack tip hydrostatic stress field, at a reference distance of $\delta_{FPZ} = 9 \mu\text{m}$ ahead of the tip for moderate-purity 2¼Cr-1Mo base plate and weld metal subjected to laboratory step cooling to promote a typical level of temper embrittlement	14

Contents

	Page	
11	Correlation between measured K_{IH} vs model-predicted concentration of H, trapped along the crack path with a binding energy, E_B , of 59 kJ/mol and in the crack tip hydrostatic stress field, at a reference distance of $\delta_{FPZ} = 9 \mu\text{m}$ ahead of the tip for moderate-purity 2¼Cr-1Mo base plate and weld metal subjected to laboratory step cooling to promote a typical level of temper embrittlement	15
12	Literature data for the effective diffusivity of H in the presence of trapping effects, D_{Eff} , for 2¼Cr-1Mo weld metal (WM SMAW and WM SAW) and base plate (MB)	19
13	Amplification of the Figure 10 correlation between measured K_{IH} and model-predicted concentration of H, $C_{T\sigma}$ ($E_B = 38 \text{ kJ/mol}$) at a reference distance of $\delta_{FPZ} = 9 \mu\text{m}$ ahead of the tip for two similar heats of moderate-purity 2¼Cr-1Mo weld metal	25
14	Schematic diagram of the H concentration profile likely to be present in a stainless steel clad Cr-Mo steel reactor wall, after programmed outgassing	26
15	Figure 10 correlation between measured K_{IH} vs model-predicted concentration of H, trapped along the crack path with a binding energy, E_B , of 38 kJ/mol and in the crack tip hydrostatic stress field, at an FPZ reference distance of $9 \mu\text{m}$ ahead of the tip for moderate-purity 2¼Cr-1Mo steel	28
16	Model-predicted critical temperature for a cracked compact tension specimen of Cr-Mo steel, fabricated from either weld metal or base plate of moderate purity and H_2 precharged to produce a homogeneously distributed total H concentration available for diffusion to the crack tip during loading	29
17	Standard Phase I compact tension specimen (1T-C, 25 mm thick) and the novel 90-mm-thick compact tension specimen employed by Japan Steel Works researchers for Phase II IHAC laboratory testing	32
18	Measured values of K_{IH} as a function of test temperature for 90-mm-thick compact tension specimens of 2¼Cr-1Mo base plate and weld metal subjected to slow-rising displacement rate at the indicated levels of dK/dt	33
19	The effect of test temperature on the extent of subcritical IHAC produced by slow-rising CMOD of 90-mm-thick compact tension specimens of H_2 -precharged 2¼Cr-1Mo Phase II weld metal (Δ , $dK/dt = 0.01 \text{ MPa}\sqrt{\text{m/s}}$)	34
20	Correlation between measured K_{IH} vs the 2-D finite element model-predicted concentration of H, trapped along the crack path with a binding energy, E_B , of 38 kJ/mol and in the crack tip hydrostatic stress field, at a reference distance of $9 \mu\text{m}$ ahead of the tip for moderate-purity 2¼Cr-1Mo base plate and weld metal	38
21	Correlation between measured K_{IH} vs the 2-D finite element model-predicted concentration of H, trapped along the crack path with a binding energy, E_B , of 38 kJ/mol and in the crack tip hydrostatic stress field, at a reference distance of $9 \mu\text{m}$ ahead of the tip for moderate-purity 2¼Cr-1Mo base plate and weld metal	39
22	Repeat of the data presented in Figure 18, intended to show that K_{IC} is very high for H-free 2¼Cr-1Mo steel, even when temper embrittled, provided that temperatures are greater than upper shelf values	40
23	Phase I steels examined showing the three broad categories of degree of temper embrittlement represented by Charpy impact FATT range for both weld metal and base plate of 2¼Cr-1Mo steel	41
24	High-purity 2¼Cr-1Mo steels examined in JIP Phase I research.	43

Contents

Page

25	Experimentally measured dependence of K_{IH} on total dissolved H concentration from high-temperature precharging in high-pressure H_2 for high-purity and laboratory step-cooled 2¼Cr-1Mo weld metal and base plate	45
26	Experimentally measured dependence of K_{IH} on total dissolved H concentration from high-temperature precharging in high-pressure H_2 for high-purity and laboratory step-cooled 2¼Cr-1Mo weld metal and base plate	45
27	Correlation between measured K_{IH} vs the concentration of H, trapped along the crack path with a binding energy, E_B , of 38 kJ/mol and in the crack tip hydrostatic stress field ($\sigma_H = 2.5\sigma_{YS}$ and $\sigma_H V_H = 2.5$ kJ/mol), at a reference distance of 9 μm ahead of the tip for modern higher-purity 2¼Cr-1Mo base plate and weld metal data presented in Figure 25	47
28	Correlation between measured K_{IH} vs the concentration of H, trapped along the crack path with a binding energy, E_B , of 38 kJ/mol and in the crack tip hydrostatic stress field ($\sigma_H = 2.5\sigma_{YS}$ and $\sigma_H V_H = 2.5$ kJ/mol), at a reference distance of 9 μm ahead of the tip for the low-FATT 2¼ Cr-1Mo base plate and weld metal data presented in Figure 26	48
29	The effect of 2¼Cr-1Mo steel purity and temper embrittlement on the critical temperature for elimination of IHAC in H_2 -precharged compact tension specimens, as a function of total precharged H concentration and based on the values of $C_{T\sigma-CRIT}$ from Figures 15 and 29	49
30	The effect of 2¼Cr-1Mo steel purity and temper embrittlement on the critical temperature defined in terms of the crack tip FPZ diffusible H concentration at $\delta_{FPZ} = 9 \mu m$, computed by a diffusion analysis and based on the values of $C_{T\sigma-CRIT}$ from Figures 15 and 28	50
31	Model prediction of critical temperature vs C_{H-Diff} at the reference location of 9 μm ahead of the crack tip, replotted from Figure 30	51
32	ABAQUS model predictions of diffusible H loss from a H_2 -precharged standard (25.4-mm-thick) compact tension specimen of 2¼Cr-1Mo steel exposed at several constant temperature and stress intensity levels	53
33	Correlation between measured K_{IH} vs the concentration of H, trapped along the crack path with a binding energy, E_B , of 3 kJ/mol and in the crack tip hydrostatic stress field ($s_H = 2.5s_{YS}$ and $s_H V_H = 2.5$ kJ/mol), at a reference distance of 470 μm ahead of the tip for modern higher-purity 2¼ Cr-1Mo base plate and weld metal data presented in Figure 25	54
34	Correlation between measured K_{IH} vs the concentration of H, trapped along the crack path with a binding energy, E_B , of 38 kJ/mol and in the crack tip hydrostatic stress field ($\sigma_H = 2.5\sigma_{YS}$ and $\sigma_H V_H = 2.5$ kJ/mol), at a reference distance of 470 μm ahead of the tip for the low-FATT 2¼Cr-1Mo base plate and weld metal data presented in Figure 26	55
35	The effect of crack tip analysis location on the predicted critical temperature for elimination of IHAC in H_2 -precharged compact tension specimens of low-FATT 2¼Cr-1Mo steel, as a function of total precharged H concentration and based on the values of $C_{TS-CRIT}$ from Figures 28 and 34	56
36	The effect of crack tip C_{H-Diff} analysis accuracy for a cracked “structure” on the predicted critical temperature for elimination of IHAC using H_2 -precharged compact tension specimens of low-FATT 2¼Cr-1Mo steel, as a function of total precharged H concentration and based on the short-term laboratory value of $C_{T\sigma-CRIT}$ from Figure 34	57

Contents

Page

37	The effect of crack tip diffusible H concentration (C_{H-Diff} 470 μm), localized at the reference point of δ_{470} μm ahead of the crack tip, on the predicted critical temperature for elimination of IHAC in a cracked section fabricated from low-FATT 2 $\frac{1}{4}$ Cr-1Mo steel, as a function of total precharged H concentration and based on the short-term laboratory value of $C_{TS-CRIT} = 1,000,000$ wppm from Figure 34	58
38	The effect of crack tip diffusible H concentration (C_{H-Diff} 470 mm), localized at the reference point of d_{470} mm ahead of the crack tip, on the predicted critical temperature for elimination of IHAC in a cracked section fabricated from moderate-FATT 2 $\frac{1}{4}$ Cr-1Mo steel, as a function of total precharged H concentration and based on the short-term laboratory value of $C_{TS-CRIT} = 117,000$ wppm taken from Figure 21 and enhanced to account for the increase in crack tip reference location from 9 mm to 470 mm	59
39	The H concentration distribution in the stainless steel clad Cr-Mo wall of a hydroprocessing reactor during: (a) operation at 450 $^{\circ}\text{C}$ in 14.7 MPa (2133 psi) H_2 , which produced $C_{H-Total} = 2.3$ wppm H in the Cr-Mo steel at the interface with the stainless cladding, and (b) after cool-down to 25 $^{\circ}\text{C}$, without H_2 present and at two rates shown by the inserted time-temperature history	60
40	REACT diffusion model output of the diffusible H concentration distribution in the stainless steel clad Cr-Mo wall of a hydroprocessing reactor during: (a) operation at 450 $^{\circ}\text{C}$ in high-pressure (unspecified) H_2 , which produced $C_{H-Diff} = 1.1$ wppm H in the Cr-Mo steel at the interface with the stainless cladding, and (b) after cool-down to 25 $^{\circ}\text{C}$, without H_2 present	61
41	The effect of total hydrogen concentration on the rising CMOD measurement of K_{IH} for JIP Phase I 2 $\frac{1}{4}$ Cr-1Mo base plate and weld metal of various purities that were temper embrittled by laboratory step cooling	64
42	3-D finite element model prediction of A_1 vs distance ahead of the crack tip along the specimen mid-thickness (top) and position along the crack front (bottom) for a standard compact tension specimen of H-precharged (initial $C_{H-Diff} = 2.0$ wppm) 2 $\frac{1}{4}$ Cr-1Mo steel that is isothermally exposed for the indicated times at 25 $^{\circ}\text{C}$. 1.0 wppm/in. $^{1/2} = 0.627$ wppm/cm $^{1/2}$	66
43	Correlation between the 2-D values of the crack tip A_1 parameter from Figure 42 (and other FEA results), and the initial diffusible H concentration (of either 2.0 or 3.25 wppm) normalized by the effective H diffusivity and exposure time for H-precharged 2 $\frac{1}{4}$ Cr-1Mo steel. 1.0 wppm/in. $^{1/2} = 0.627$ wppm/cm $^{1/2}$	67
44	Correlation between K_{IH} and $\phi = A_1 \exp(2000/T)$, where all data are reproduced from the JIP Phase I and Phase II results presented in Figure 10 for mid-FATT H precharged 2 $\frac{1}{4}$ Cr-1Mo steel. 1.0 wppm/in. $^{1/2} = 0.627$ wppm/cm $^{1/2}$	68
45	Correlation between K_{IH} and $\phi = A_1 \exp(2000/T)$ with temperature in degrees K for limited data reported for a modern low-FATT base plate of 2 $\frac{1}{4}$ Cr-1Mo steel, which is a subset of the large data base presented in Figure 26. 1.0 wppm/in. $^{1/2} = 0.627$ wppm/cm $^{1/2}$	69
46	FEA mesh for H diffusion analysis associated with an ID crack in a stainless steel clad Cr-Mo reactor vessel in elevated-temperature, high-pressure H_2 service, including the shutdown and startup time-temperature profile in the inset.	71

Contents

	Page
47 Diffusible H concentration, represented by the A_1 parameter, vs distance from the tip of an ID surface crack located either (top) 5.4 mm or (bottom) 23.7 mm inward from the pressure vessel ID surface based on REACT FEA for the conditions shown in Figure 46 and results shown in Figure 40. λ is 0.88 (Figure 43), $D_{Eff} = 1.0 \times 10^{-6} \text{ cm}^2/\text{s}$, and $C_{H-Diff} = 0.65 C_{H-Total} \cdot 1.0 \text{ wppm}/\text{in.}^{1/2} = 0.627 \text{ wppm}/\text{cm}^{1/2}$	72
48 The operating-time dependence of the H concentration similitude parameter, ϕ , for two crack depths in a stainless steel clad Cr-Mo reactor vessel subjected to the shutdown and startup cycle shown in Figure 46	73
49 The predicted operating-time dependence of MPT, defined by the ratio of constant critical ϕ (selected parametrically) to A_1 from FEA of the cracked pressure vessel represented in Figures 46 and Figure 47 for a single crack depth	73
50 Predictions of the AG model showing the effect of crack tip diffusible H concentration ($C_{H-Diff} 470 \mu\text{m}$), localized at the reference point of $\delta_{470 \mu\text{m}}$ ahead of the crack tip, on the predicted critical temperature for elimination of IHAC in a cracked section fabricated from low-FATT 2¼Cr-1Mo steel, as a function of total precharged H concentration and based on the short-term laboratory value of $C_{T\sigma-CRIT} = 1,000,000 \text{ wppm}$ from Figure 34	75
51 Comparison of experimental and Gerberich-model-predicted values of threshold stress intensity factor, typically K_{TH} for the steels investigated, as a function of the reversibly trapped and stress enhanced H concentration adjacent to the crack path	77
52 Blind prediction of K_{TH} for Cr-Mo steel using: (a) uniformly dissolved $C_{H-Total}$ available for diffusion to the $470 \mu\text{m}$ reference location, followed by partition to the crack tip stress field and trapping at sites adjacent to the IHAC path, (b) average values of all model parameters for the 300 to 700 MPa yield strength steels shown in Figure 51 and Table 6, and (c) at 25 °C	79
53 The effect of measured total H concentration ($C_{H-Total}$) on K_{IH} for the onset of IHAC under rising CMOD ($dK/dt = 0.007 \text{ MPa}\sqrt{\text{m}}$) for 2¼Cr-1Mo base plate and weld metal of several purity levels, laboratory step cooled to simulate temper embrittlement and IHAC tested at 25 °C	80
54 Comparison of measured K_{TH} for moderate-purity temper embrittled Cr-Mo steel (red trend line from Figure 53 for step-cooled specimens) with micromechanical model results (blue dotted line)	81
55 Comparison of measured K_{TH} for moderate-purity Cr-Mo steel (red trend line from Figure 53 for step-cooled temper embrittled specimens) with micromechanical model results (blue dotted line) for the H concentration located at $d_{FPZ} = 9 \text{ mm}$	82
56 Comparison of measured K_{TH} for high-purity Cr-Mo steel (red trend line from Figures 25 and 26 for step-cooled specimens) with micromechanical model results (blue dotted line)	83
57 Comparison of measured K_{TH} for high-purity Cr-Mo steel (red trend line from Figures 25 and 26 for step-cooled specimens) with micromechanical model results (blue dotted line) for the H concentration located at $\delta_{FPZ} = 9 \mu\text{m}$	84
58 Calibrated prediction of K_{IH} for high-purity Cr-Mo weld metal and base plate as a function of the concentration of stress field and crack path trap site enhanced H concentration, $C_{T\sigma}$, at the $9 \mu\text{m}$ crack tip reference location	85
59 Calibrated prediction of K_{TH} for moderate-purity temper embrittled Cr-Mo weld metal and base plate plotted as a function of the concentration of stress field and crack path trap site enhanced H concentration, $C_{T\sigma}$, at the $9 \mu\text{m}$ crack tip reference location	87

Contents

	Page	
60	Alternate best fit prediction of measured K_{TH} for moderate-purity temper embrittled Cr-Mo steel (red trend line from Figure 53 for step-cooled temper embrittled specimens) with micromechanical model results (blue dotted line) for the H concentration located at $\delta_{FPZ} = 9 \mu\text{m}$	88
61	Alternate prediction of K_{TH} for moderate-purity Cr-Mo steel as a function of the concentration of stress field and crack path trap site enhanced H concentration, $C_{T\sigma}$, computed using the model parameters fit to the K_{IH} vs uniformly dissolved initial total H concentration, $C_{H-Total}$, represented in Figures 53 and 60, and Task 1.0 master correlation value of E_B (38 kJ/mol)	89
62	Calibrated fit prediction of K_{TH} for moderate-purity temper embrittled Cr-Mo weld metal and base plate plotted as a function of the concentration of stress field and crack path trap site enhanced H concentration, C_{TS} , at the 9 mm crack tip reference location.	90
63	Schematic representation of model-predicted master correlations for four temperatures, e.g. from left to right: 400 K (red), 343 K (green), 298 K (blue), and 250 K (orange) inspired by the quantitative predictions shown in Figure 62	91

Tables

1	Definition of the Trap-affected H Diffusivity vs Temperature, Diffusible H Concentration, and Plastic Deformation at the Crack Tip of 2.25Cr-1Mo Weld Metal ($\sigma_{YS} = 508 \text{ MPa}$) for FEA Diffusion Modeling Using ABAQUS	18
2	Estimated Stress-enhanced Diffusible H near the Crack Tip from the 3-D Fixed K Diffusion Model to Approximate the Effect of dK/dt . $D_H = f(C_H, T, \epsilon_P)$	21
3	Estimated Stress-enhanced Normalized Diffusible H [$C_{H-Diff-\sigma} / C_{H-Diff-Bulk}(t=0)$] at the Crack Tip of H_2 -precharged Standard Compact Tension from the 3-D Fixed K Diffusion Model to Approximate the Effect of Slowly Rising Load at a dK/dt of $0.007 \text{ MPa}\sqrt{\text{m/s}}$. $D_H = f(C_H, T, \epsilon_P)$	22
4	2-D Diffusion Model Prediction of Peak Diffusible H Concentration near the Crack Tip for Standard and Slotted Compact Tension Specimens As a Function of Stress, Time, and Temperature. $D_H = f(C_H, T, \epsilon_P)$	35
5	Comparison Between 2-D and 3-D Hydrogen Diffusion Model Predictions	36
6	Parameters Used to Predict Threshold Stress Intensity Factor for IHAC in Steels of Varying Tensile Yield Strength Using Gerberich's Decohesion Model.	77

EXECUTIVE SUMMARY

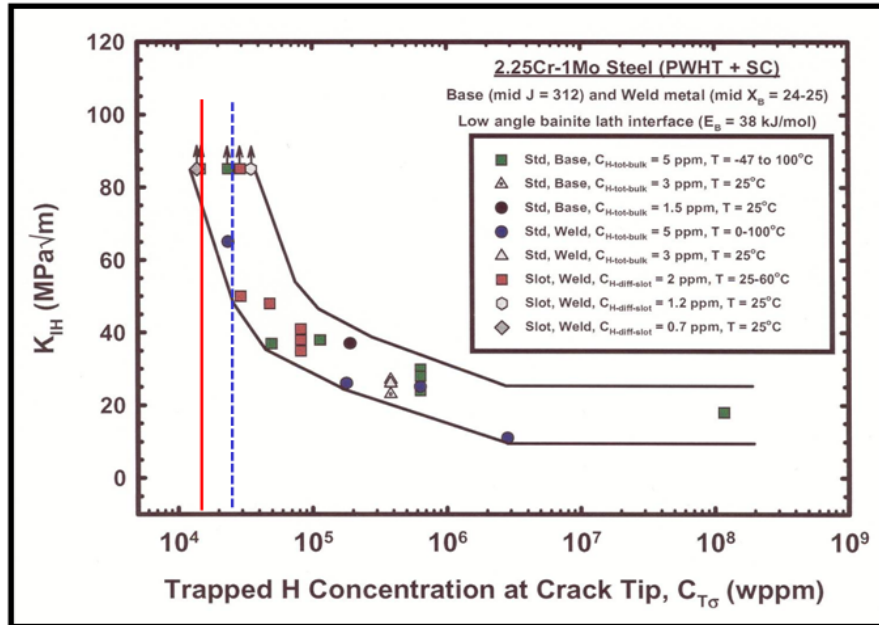
The objective of this study, in support of API Recommended Practice 934-F [*Guidance for Establishing a Minimum Pressurization Temperature (MPT) for Heavy Wall Reactors in High Temperature Hydrogen Service During Startups and Shutdowns*], is to establish the technical basis for determining a minimum pressurization temperature (MPT) necessary to avoid internal hydrogen-assisted cracking (IHAC) of weld metal and base plate of temper embrittled 2¼Cr-1Mo steel in high-pressure H₂ service. The threshold condition for the onset of subcritical crack propagation—and its dependencies on dissolved hydrogen concentration, temperature, and steel purity/temper embrittlement—are targeted as particularly important to pressure vessel safe operations. A second objective is to improve the underlying data base for fracture mechanics fitness-for-service (FFS) modeling of IHAC. Both analyses are built on the conservative rising displacement threshold stress intensity factor for IHAC (K_{IH}).

This investigation has accomplished five tasks, leading to the following conclusions and key figures taken from the body of this report. These conclusions are sufficient to establish the API 934-F section on MPT to conservatively avoid IHAC in 2¼Cr-1Mo steel.

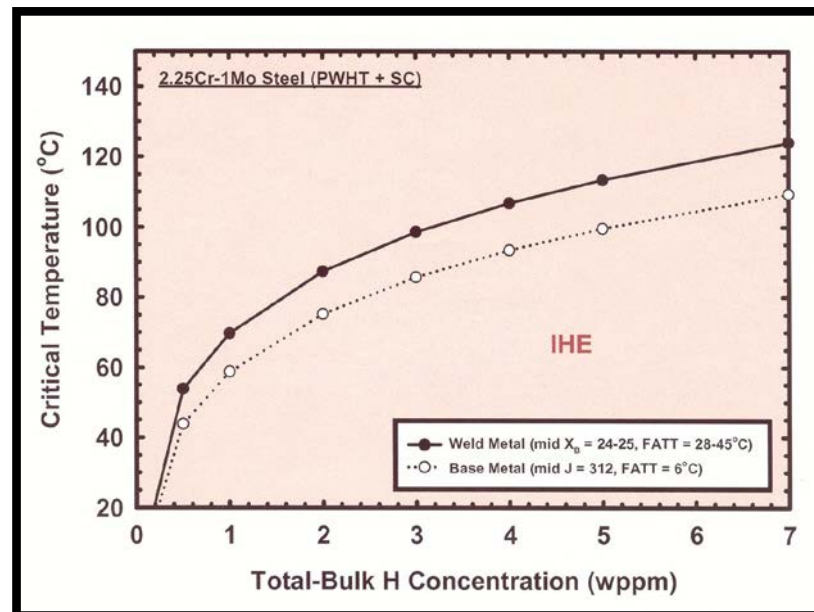
Task 1.0—Summarize and clarify the technical approach, assumptions, data, and modeling results used in Phase II JIP research to quantitatively establish the H concentration and temperature dependencies of the threshold stress intensity, K_{IH} , for IHAC and the concentration dependence of MPT for moderate-impurity 2¼Cr-1Mo steel.

- 1) Measured threshold stress intensity factor (K_{IH}) for the onset of IHAC increases with decreasing bulk-dissolved H concentration and increasing temperature, as proved by experimental results for multiple specimen geometries of 2¼Cr-1Mo steel.
- 2) The H concentration and temperature dependencies of K_{IH} are explained physically by the interactive effect of each variable on the concentration of H ($C_{T\sigma}$) that is enhanced at a reference location in the crack tip fracture process zone due to localized hydrostatic stress and microstructure sites for H trapping that constitute the crack path.
- 3) The steps necessary to predict $C_{T\sigma}$ as a function of total dissolved H concentration and temperature, proposed by Al-Rumaih in a joint industry program (JIP) Phase II PhD study at the University of Virginia, are validated as fully correct and are clarified to provide the scientific basis for engineering applications that seek to avoid IHAC. This analysis was guided by mechanistic consideration of H trapping and embrittlement in the crack tip region of a complex steel microstructure.

- 4) A master experimental correlation exists between measured K_{IH} and diffusion-model-predicted $C_{T\sigma}$ for moderate-purity temper embrittled [$6\text{ }^\circ\text{C} < \text{fracture appearance transition temperature (FATT)} < 43\text{ }^\circ\text{C}$] 2¼Cr-1Mo, including a critical level of locally trapped H below which K_{IH} rises toward K_{IC} ($C_{T\sigma\text{-CRIT}}$). The critical H concentration is marginally lower for weld metal compared to base plate, with each microstructure temper embrittled by laboratory step cooling. Figure 15 follows, specific to $C_{T\sigma}$ predicted at 2CTOD ahead of the crack tip; $\delta_{FPZ} = 9\text{ }\mu\text{m}$:

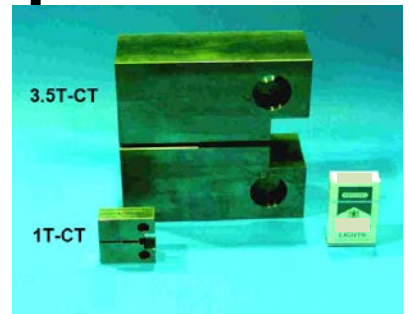
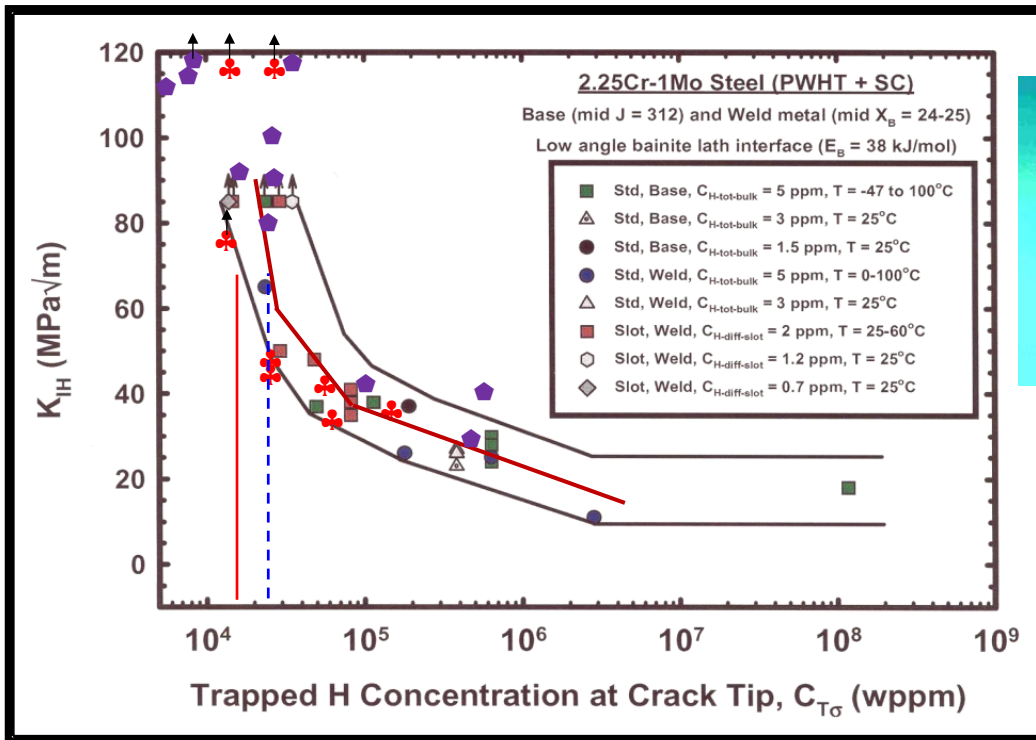


- 5) The master K_{IH} vs $C_{T\sigma}$ correlation provides the basis for a critical temperature, T_{CRIT} , above which IHAC is not observed and that is the foundation for MPT determination. The T_{CRIT} increases with increasing $C_{H\text{-Total}}$ dissolved in the "structure" at high temperature, with a quantitative dependence reported in Phase II work specific to the compact tension geometry and moderate-FATT 2¼Cr-1Mo weld metal and base plate. Figure 16 follows based on K_{IH} vs $C_{T\sigma}$ in Figure 15. Diffusion analysis (see Task 4.0) is required to apply this specific result to a cracked reactor vessel in H_2 service.



Task 2.0—Validate the Phase II correlation of K_{IH} and critical temperature vs H concentration, based on new analyses of post-Phase-II IHAC data.

- Japanese experiments with unusually thick and H_2 -precharged compact tension specimens of moderate-purity temper embrittled $2\frac{1}{4}Cr-1Mo$ weld metal and base plate ($22\text{ }^\circ\text{C} < \text{FATT} < 43\text{ }^\circ\text{C}$) quantitatively validate the master correlation between K_{IH} and $C_{T\sigma}$. Figure 21 follows showing agreement between these thick-specimen results (\clubsuit, \spadesuit) and the small-specimen master curve from Figure 15, each related to $\delta_{FPZ} = 9\text{ }\mu\text{m}$:



Task 3.0—Enhance the Phase II analysis of K_{IH} vs crack tip H concentration, and thus MPT, by describing the interaction between temper embrittlement and IHAC using JIP Phase I data so as to predict the influence of modern steel purity.

- Results of extensive JIP Phase I IHAC experiments, conducted with H_2 -precharged compact tension specimens of multiple high-purity lots of laboratory step-cooled $2\frac{1}{4}Cr-1Mo$ weld metal and base plate ($-90\text{ }^\circ\text{C} < \text{FATT} < -28\text{ }^\circ\text{C}$) are well correlated by a master correlation between K_{IH} and $C_{T\sigma}$, as verified by additional literature K_{IH} data.